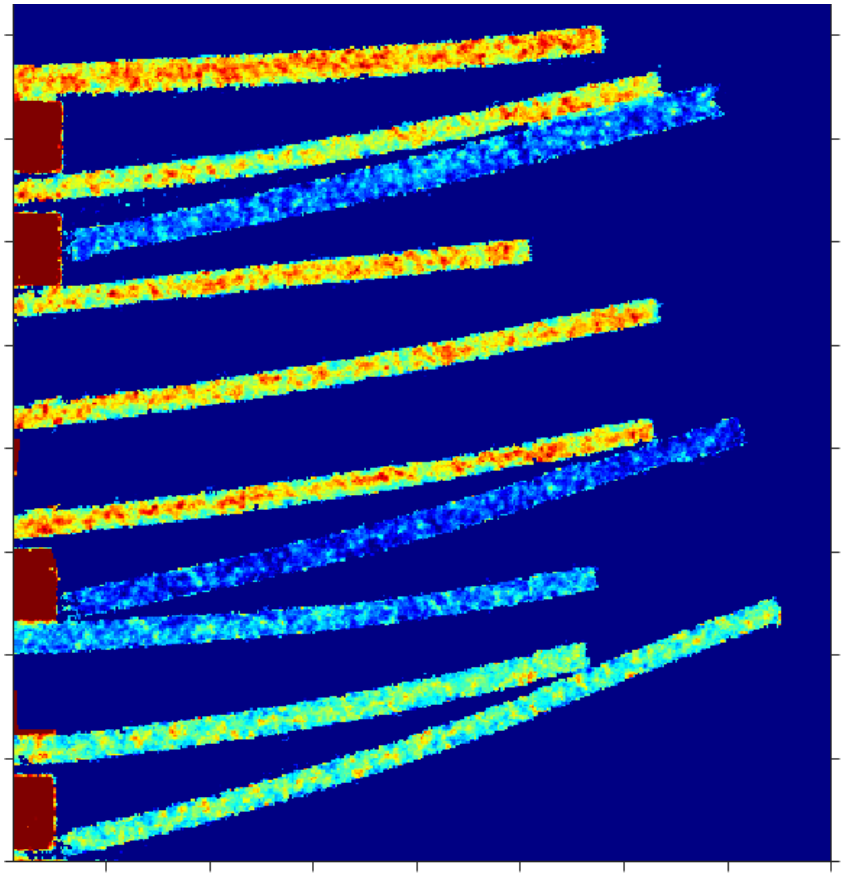

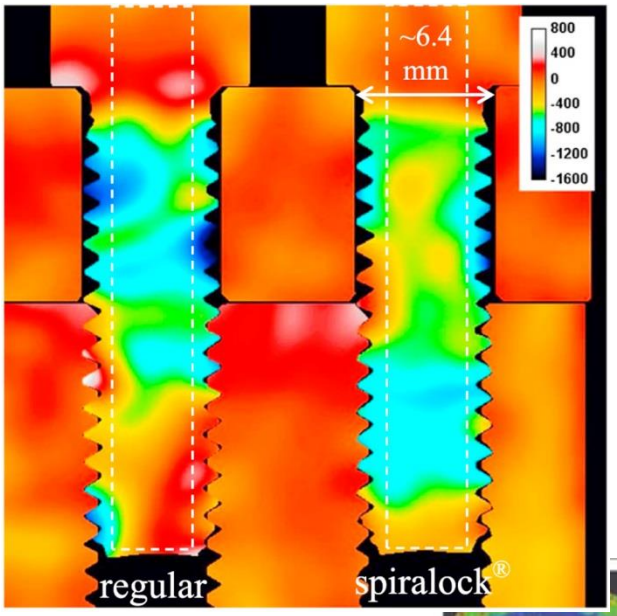

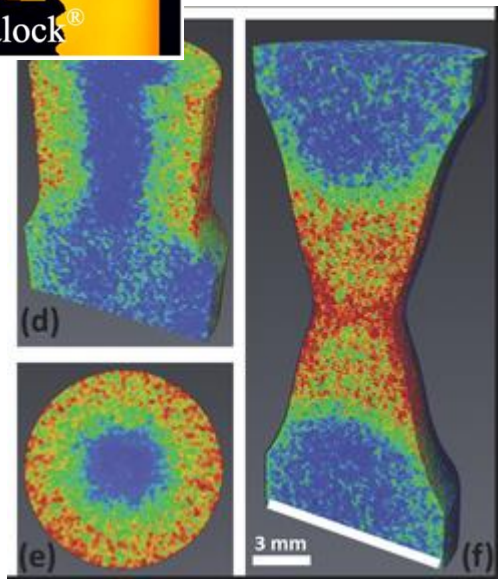

Bragg edge neutron imaging

Malgorzata Makowska

Outline

- Bragg edge imaging – principles
- Pulsed vs continuous neutron flux
- Aplications
- Data analysis

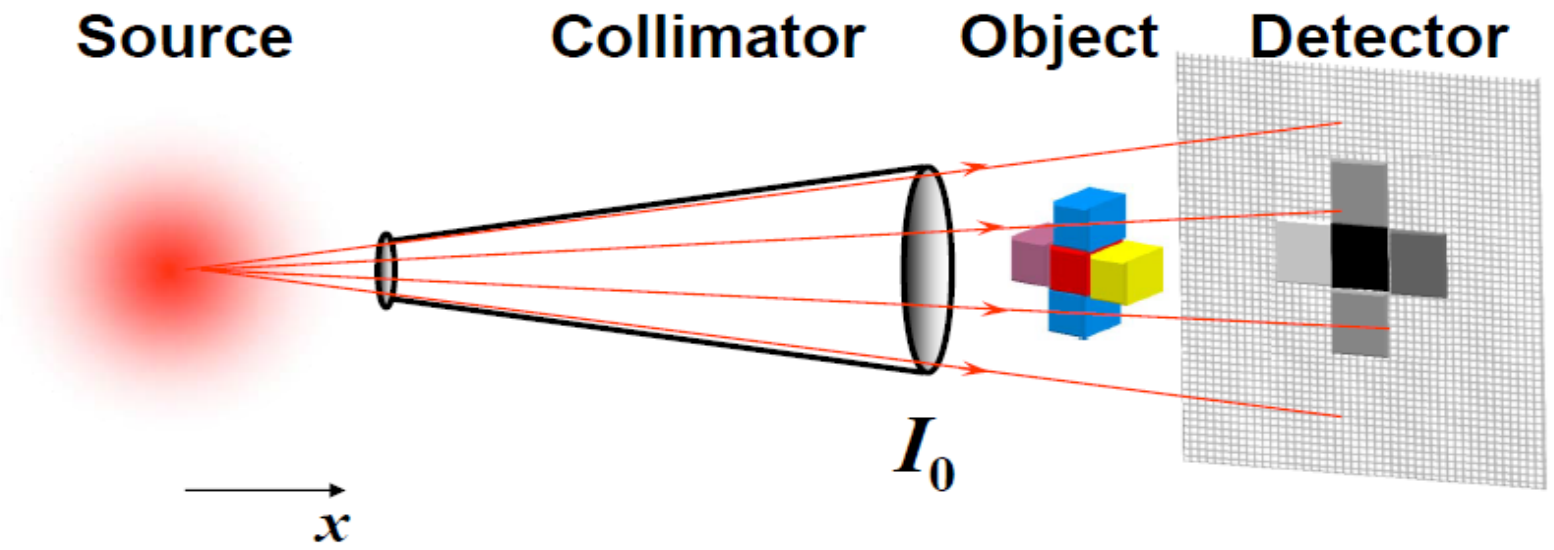

$$\sim I_0 e^{-\int \mu(x)dx}$$

x – propagation direction

I_0 – primary beam

$\mu(x)$ – attenuation coefficient

Strobl, M. et al. (2009). *J. Phys. D. Appl. Phys.* **42**, 243001.

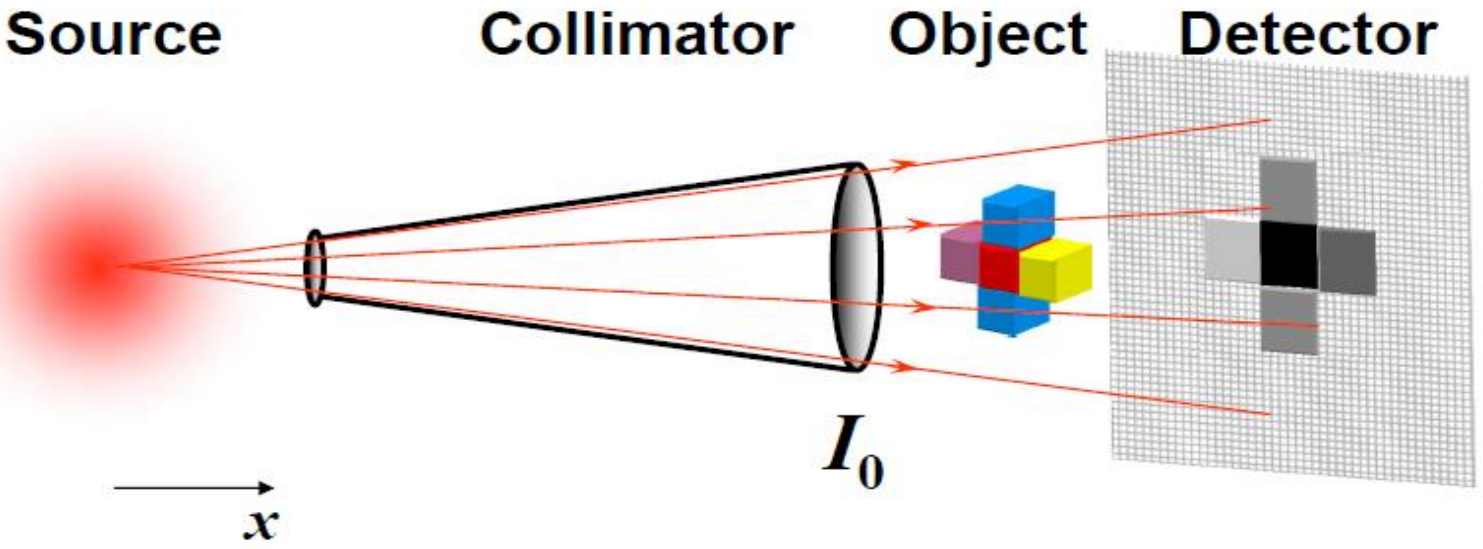

$$\sim I_0 e^{-\int \mu(x,\lambda)dx\, d\lambda}$$

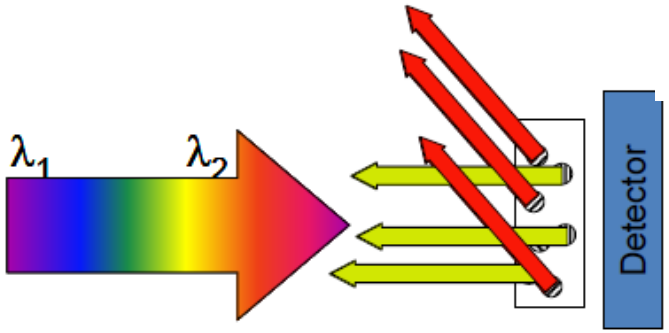

Neutron cross section components

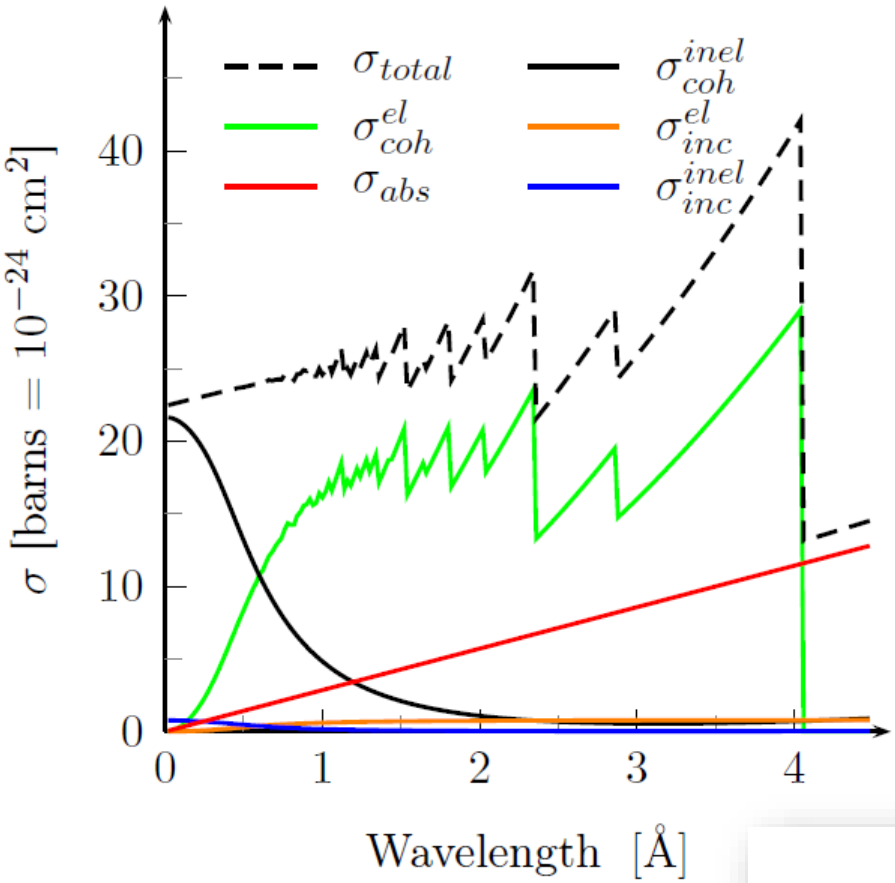

M. Boin, PhD thesis

Macroscopic neutron cross section:

$$\mu(\lambda)=n\sigma$$

n – concentration of centers interacting with neutrons

Microscopic neutron cross section:

$$\sigma_{total} = \sigma^{inel}_{coh} + \sigma^{inel}_{incoh} + \sigma^{el}_{coh} + \sigma^{el}_{incoh} + \sigma_{abs}$$

X RAYS
AND
CRYSTAL STRUCTURE

BY

W. H. BRAGG, M.A., D.Sc., F.R.S.
CAVENDISH PROFESSOR OF PHYSICS, UNIVERSITY OF LEEDS
AND
W. L. BRAGG, B.A.
FELLOW OF TRINITY COLLEGE, CAMBRIDGE

LONDON
G. BELL AND SONS, LTD.
1915

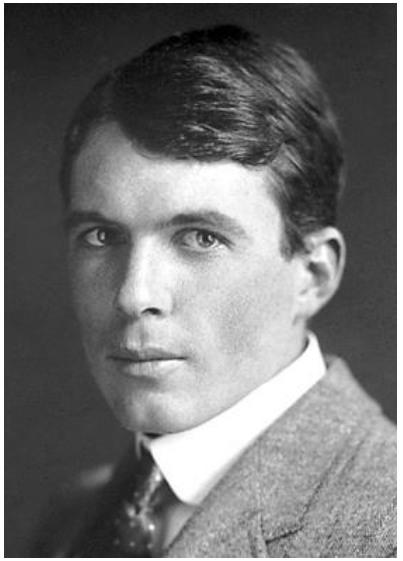

William Lawrence Bragg

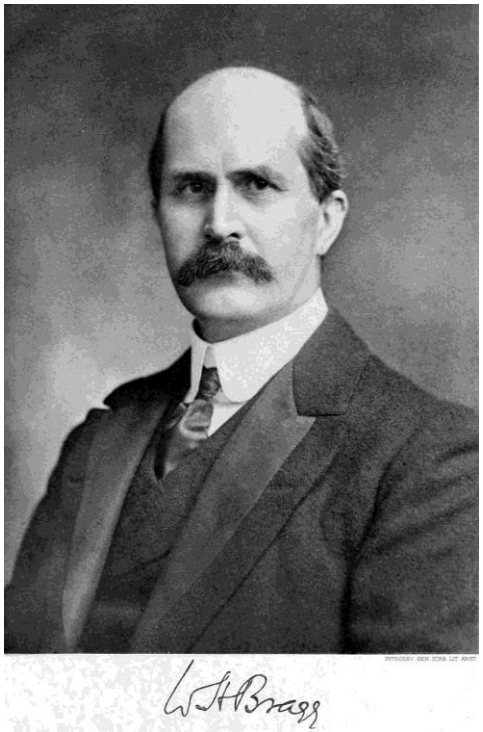

Sir William Henry Bragg

Bragg‘s law

“We find the angle at which a monochromatic beam of X-rays of known wavelength is reflected by the various faces of the crystal. Reflexion takes place only when the relation

$$n\lambda = d \sin\theta$$

is satisfied, and so the spacing d of the planes parallel to any face under examination can be found by measuring the angle θ…. “

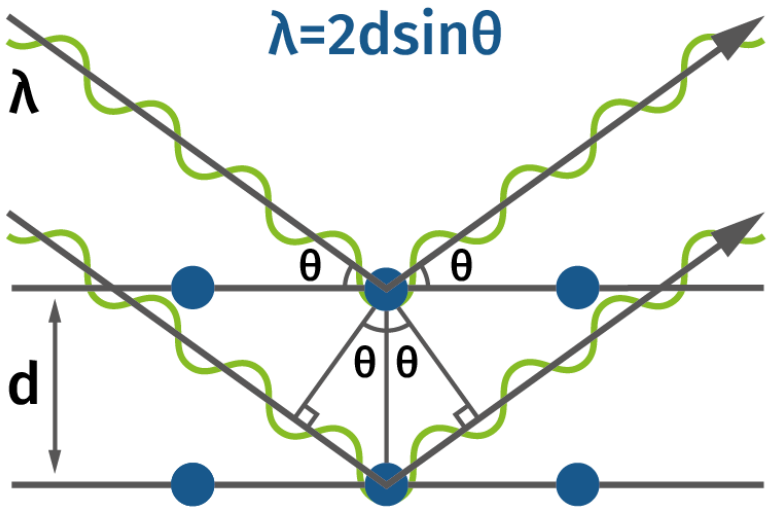

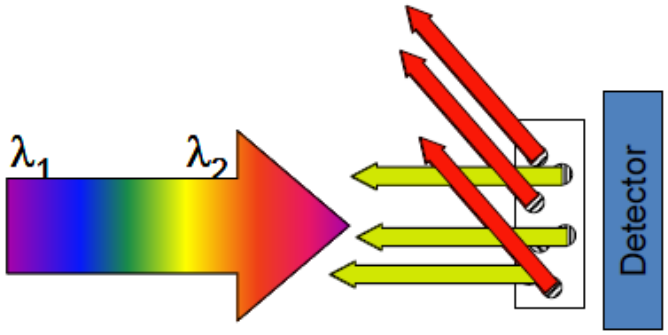

Bragg's law:

$2d_{hkl}\sin\theta=\lambda$

$2d_{hkl}\sin 90^\circ=\lambda$

$2d_{hkl}\sin\theta< \lambda$

Total neutron cross section for different polycrystalline materials

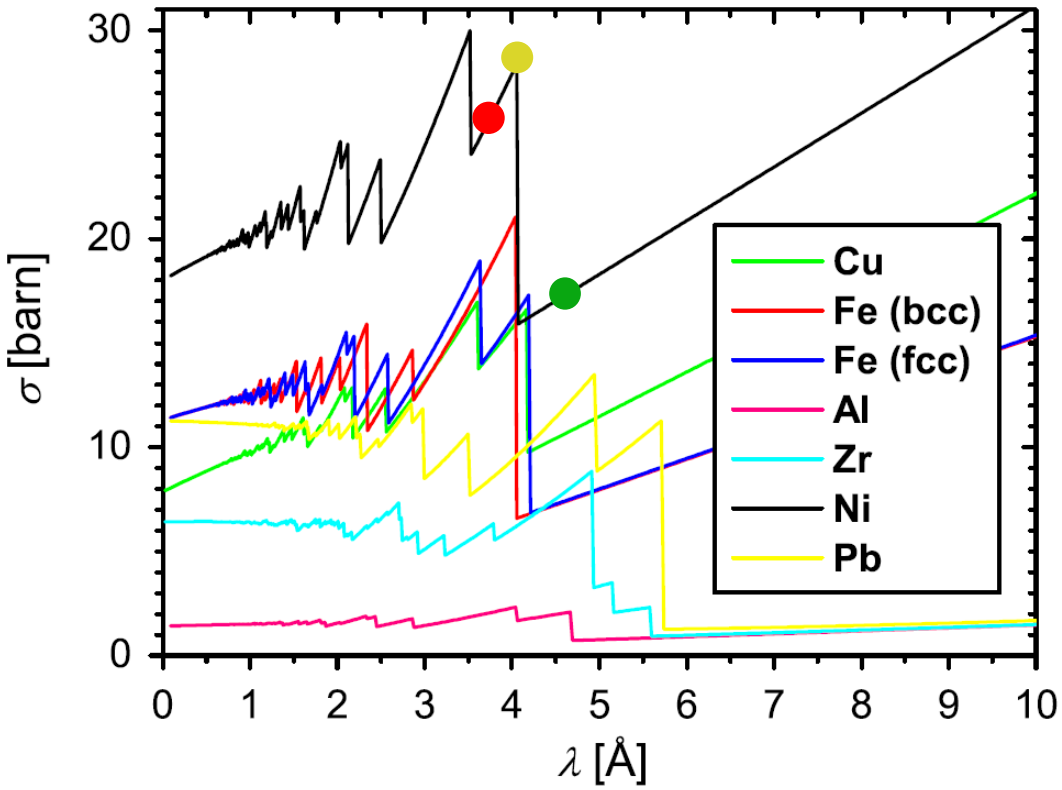

Josic, L., Lehmann, E., & Kaestner, a. (2011). Nucl. Instruments Methods Phys. Res. 651, 166–170.

Total coherent elastic cross section for isotropic polycrystal:

$$\sigma^{el}{}_{coh} = \frac{\lambda^2}{4V_0} \sum_{hkl}^{2d_{hkl}<\lambda} |F_{hkl}|^2 d_{hkl}$$

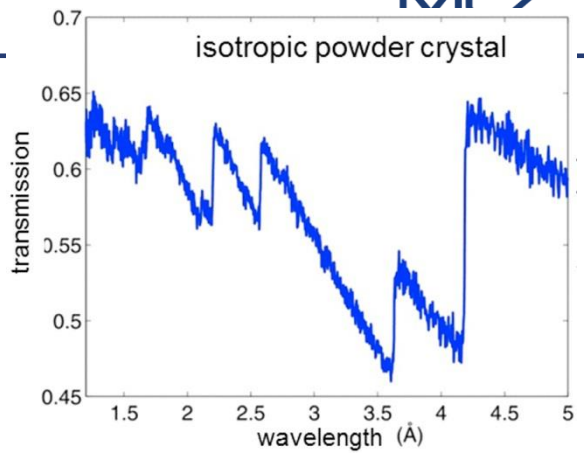

Total coherent elastic cross section for textured crystal:

$$\sigma^{el}{}_{coh} = \frac{\lambda^2}{4V_0} \sum_{hkl}^{2d_{hkl}<\lambda} |F_{hkl}|^2 d_{hkl}\, R(\psi, \lambda, d_{hkl})$$

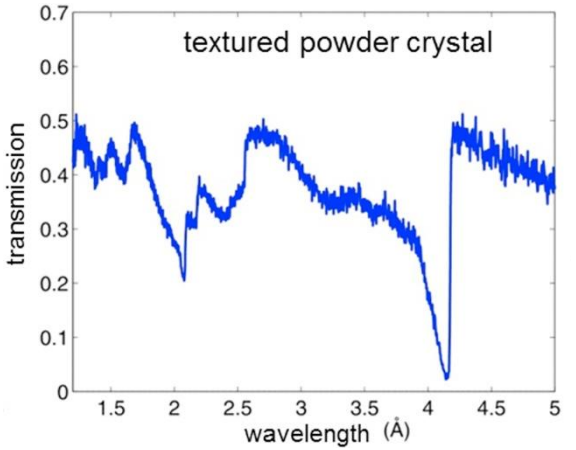

Total coherent elastic cross section for single crystal:

$$\sigma^{el}{}_{coh} = \sum_{hkl} y_{hkl} \frac{|F_{hkl}|^2 \lambda_{hkl}{}^4}{2V_0 \sin^2\theta_{hkl}} P(\lambda_{hkl}, \varpi_{hkl}, \lambda)$$

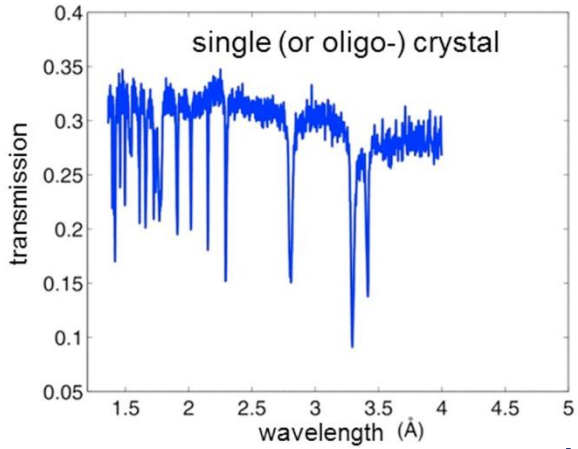

Energy resolved neutron imaging at continuous sources

- Neutron source
- Monochromator (double crystal monochromator or/and velocity selector)
- Detector

Energy resolved neutron imaging at pulsed neutron sources

- Neutron source
- Detector

Energy resolved neutron imaging at pulsed neutron sources

- time of flight (TOF) approach

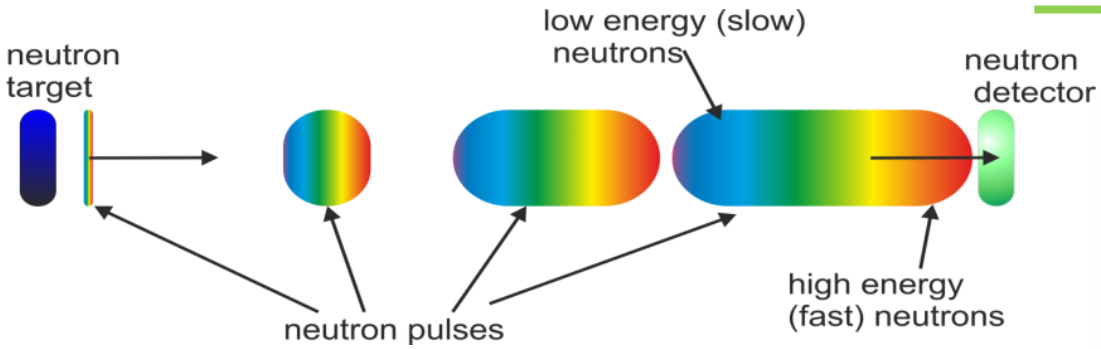

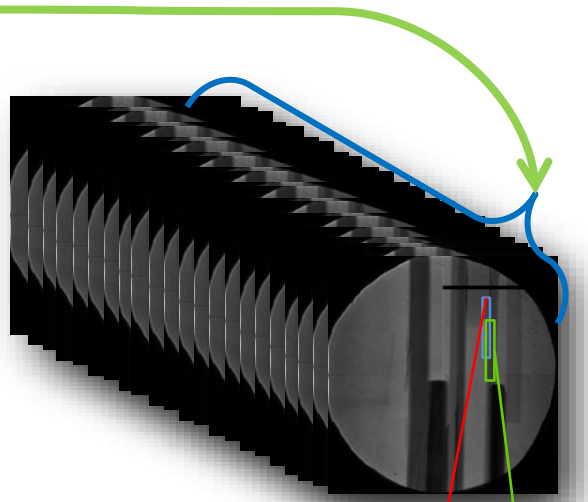

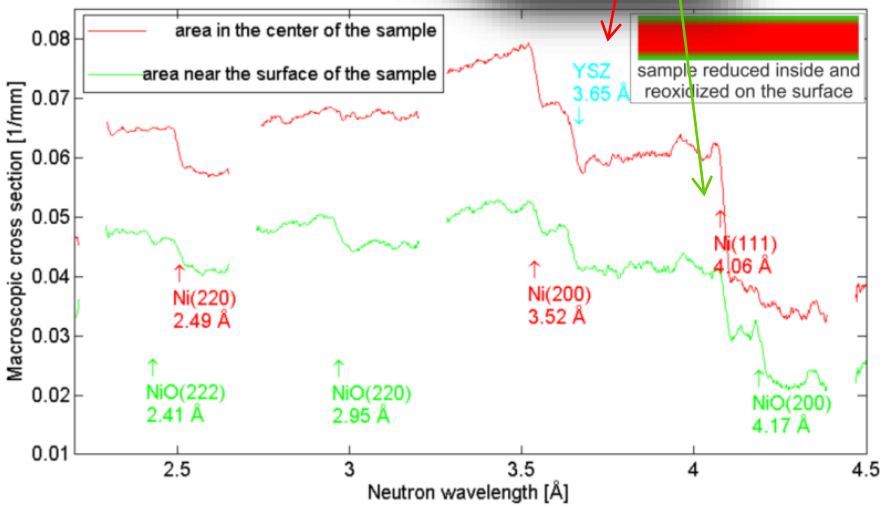

Energy resolved neutron imaging at continuous neutron sources

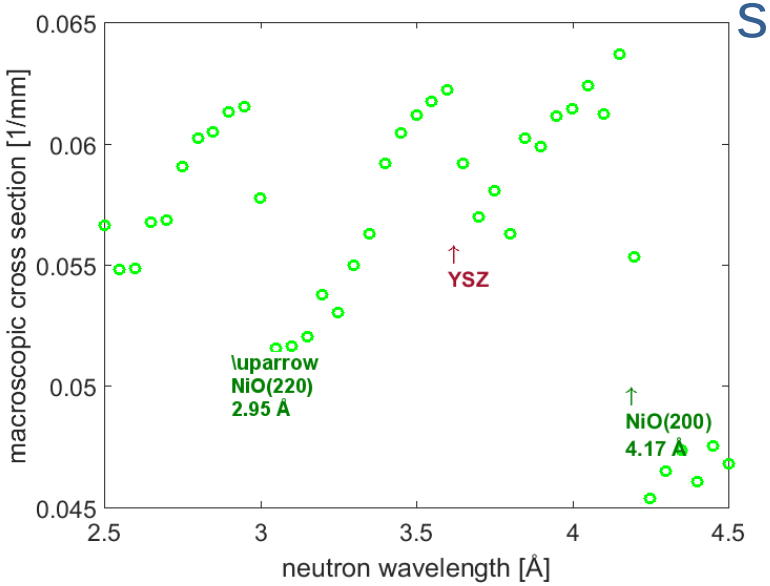

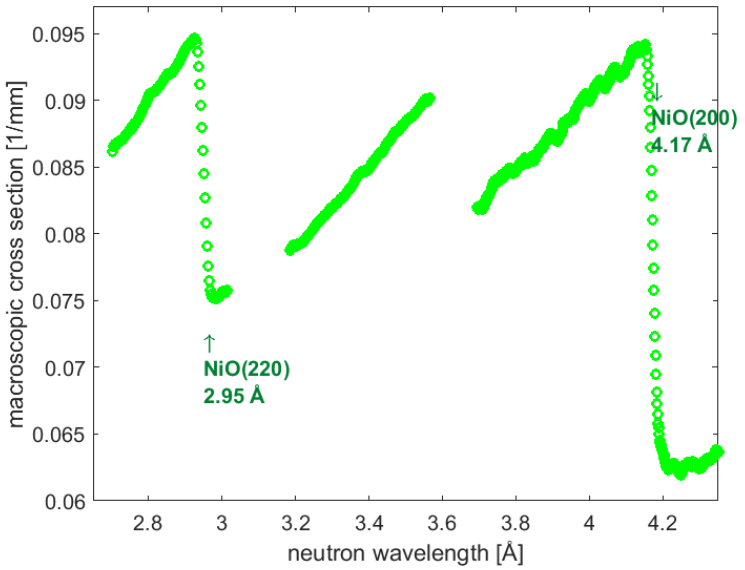

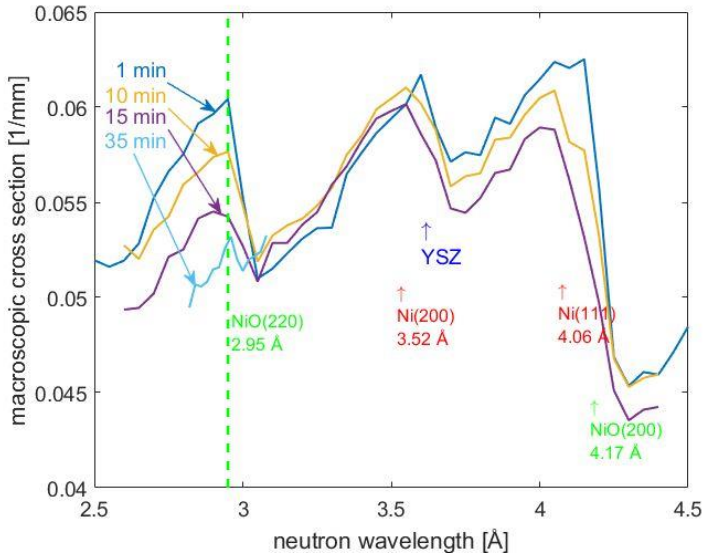

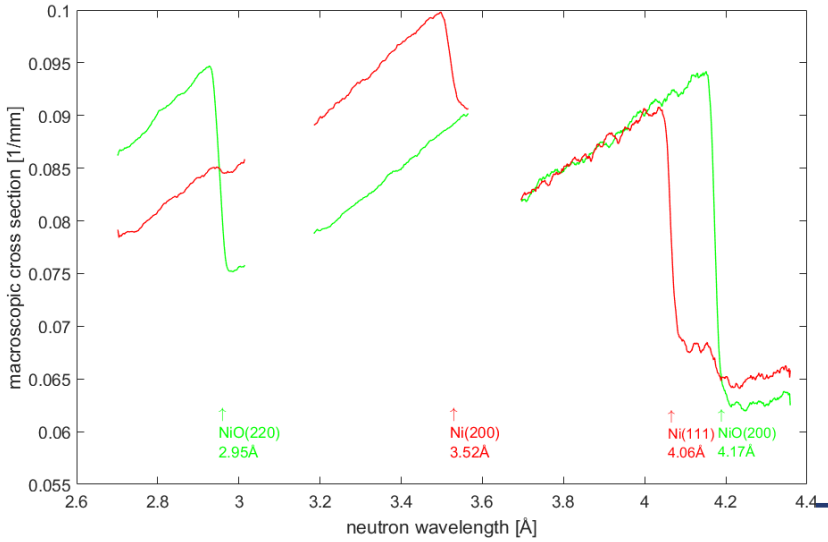

In-situ neutron imaging of phase transition at continues neutron sources using monochromatic beam

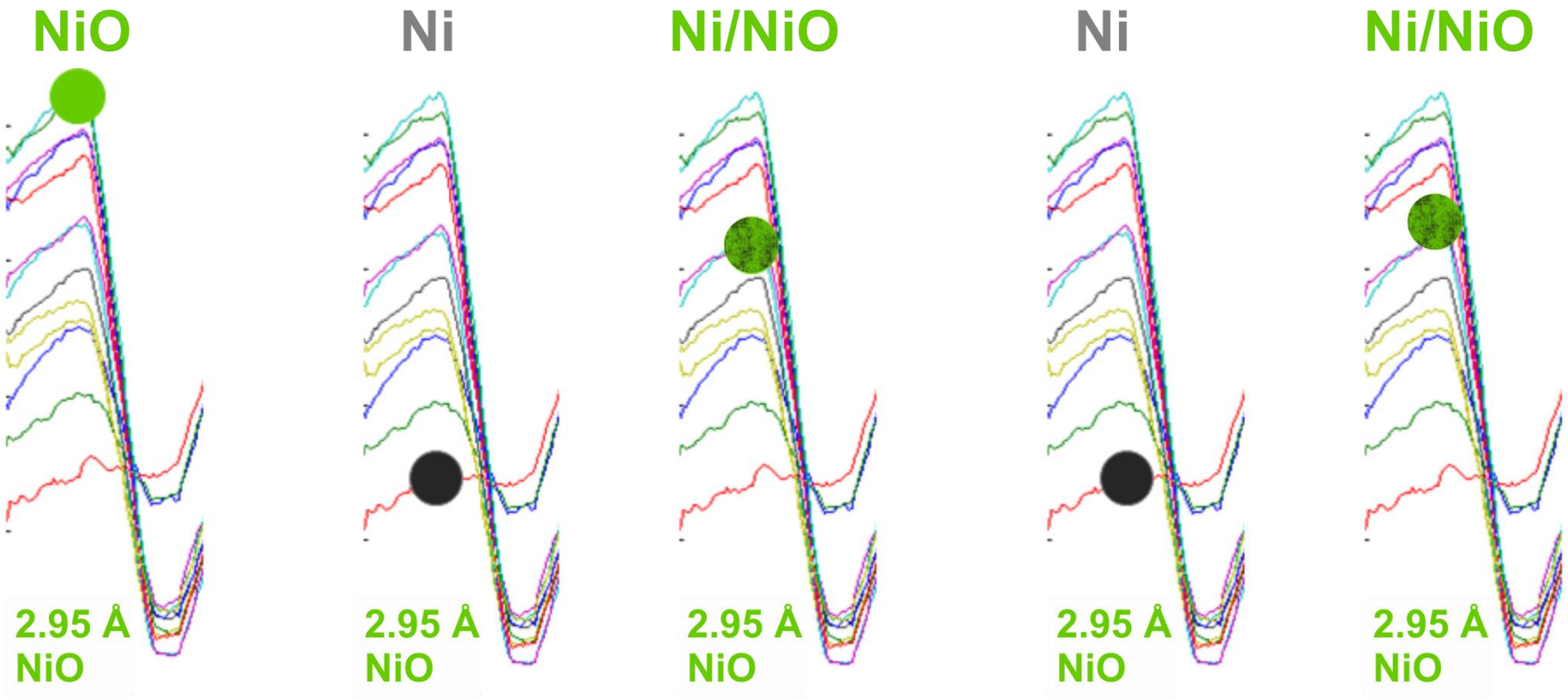

Applications

- Phase mapping
- Stress / strain mapping
- Texture analysis
- Grain reconstruction

TOF

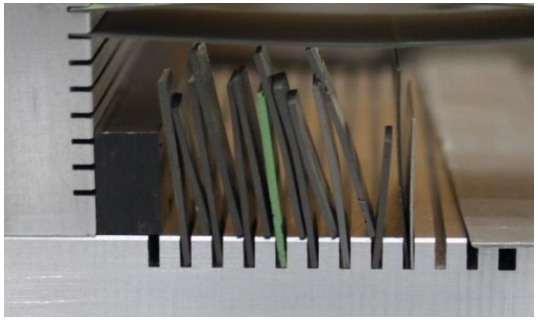

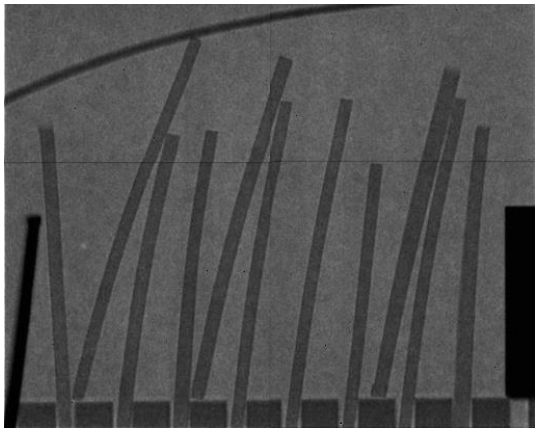

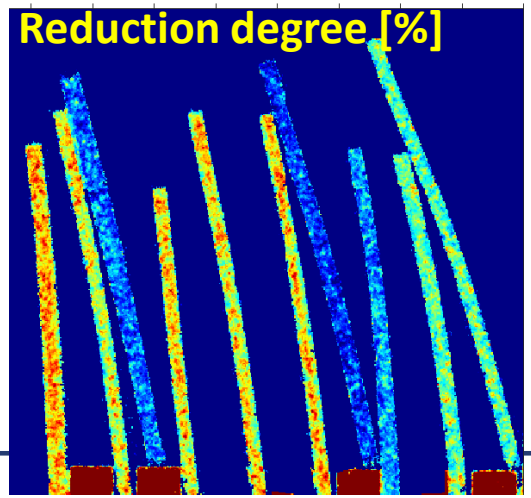

Bragg edge patterns for anode supports with different reduction degree

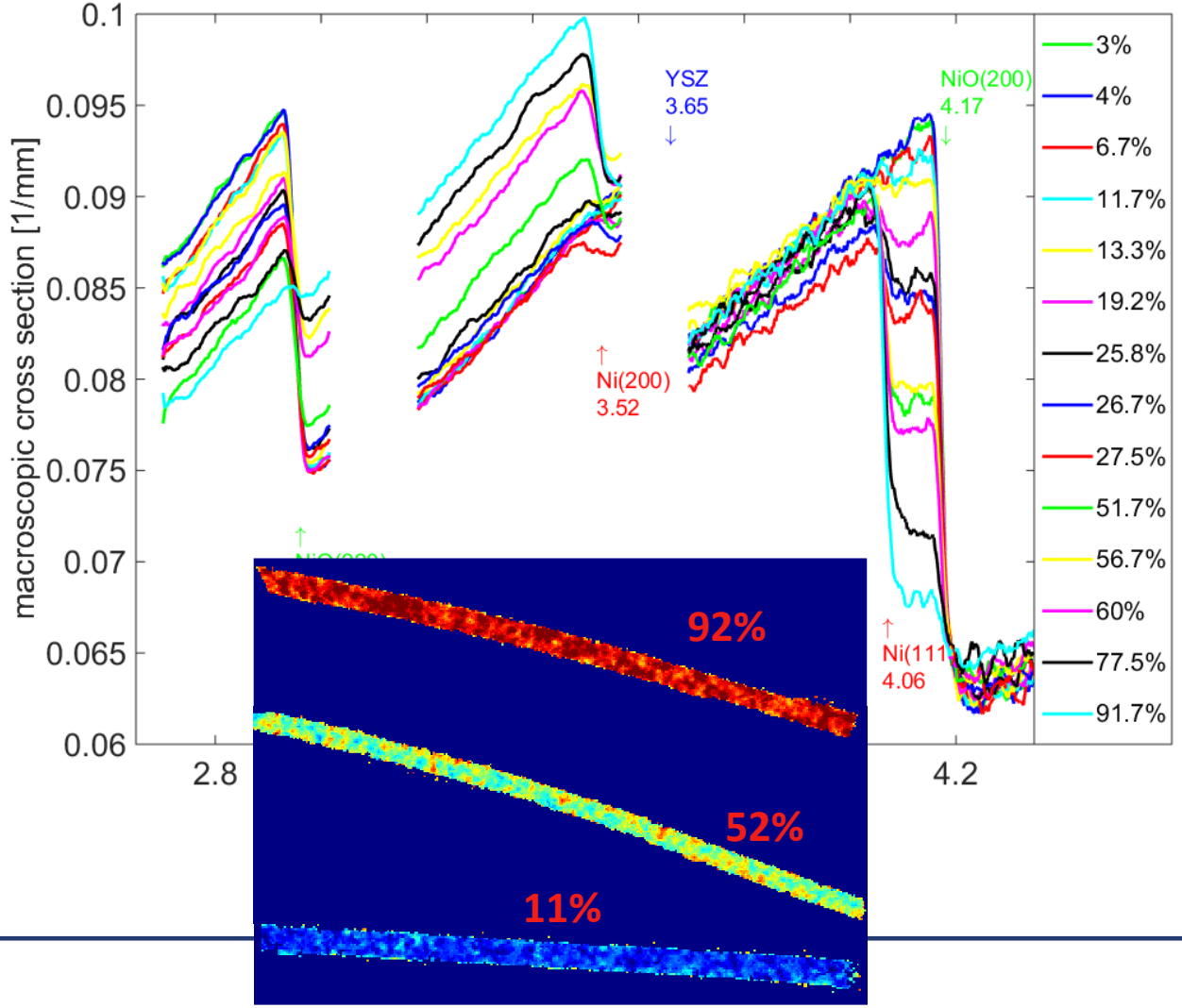

3D monochromatic neutron imaging

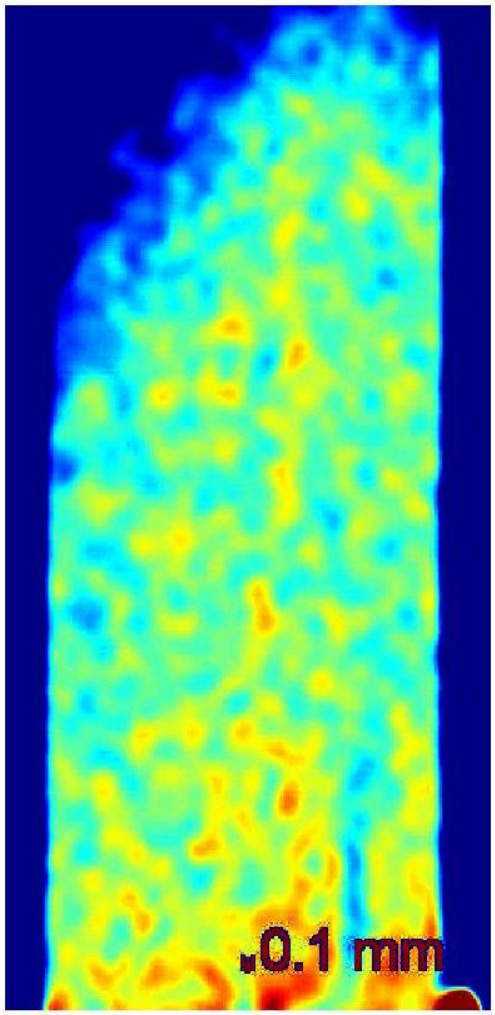

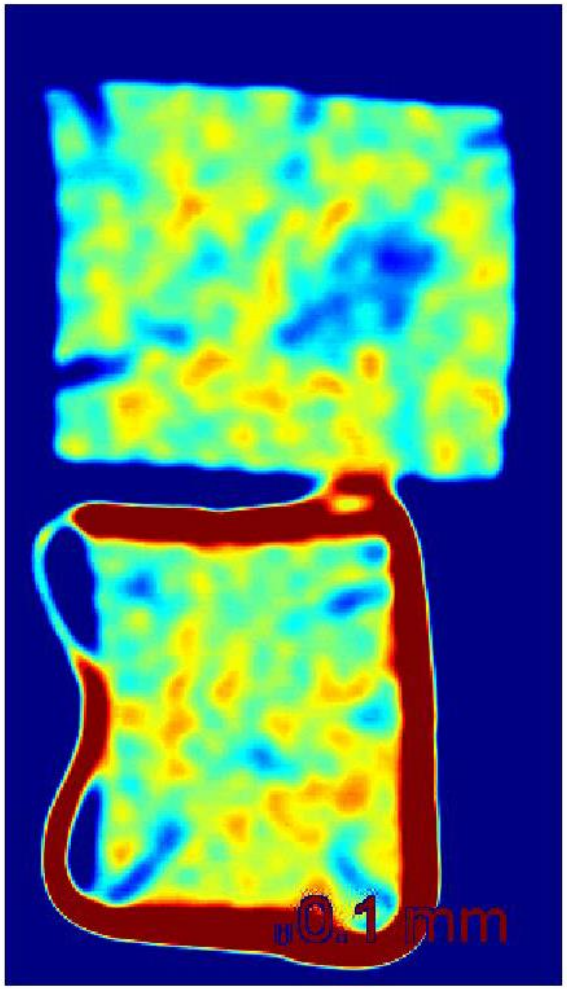

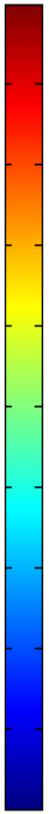

NiO

Ni

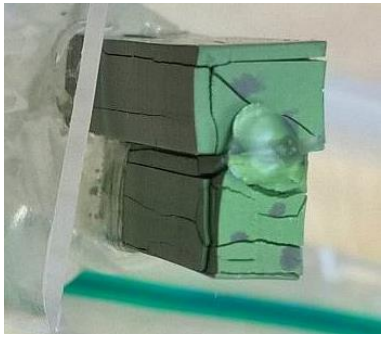

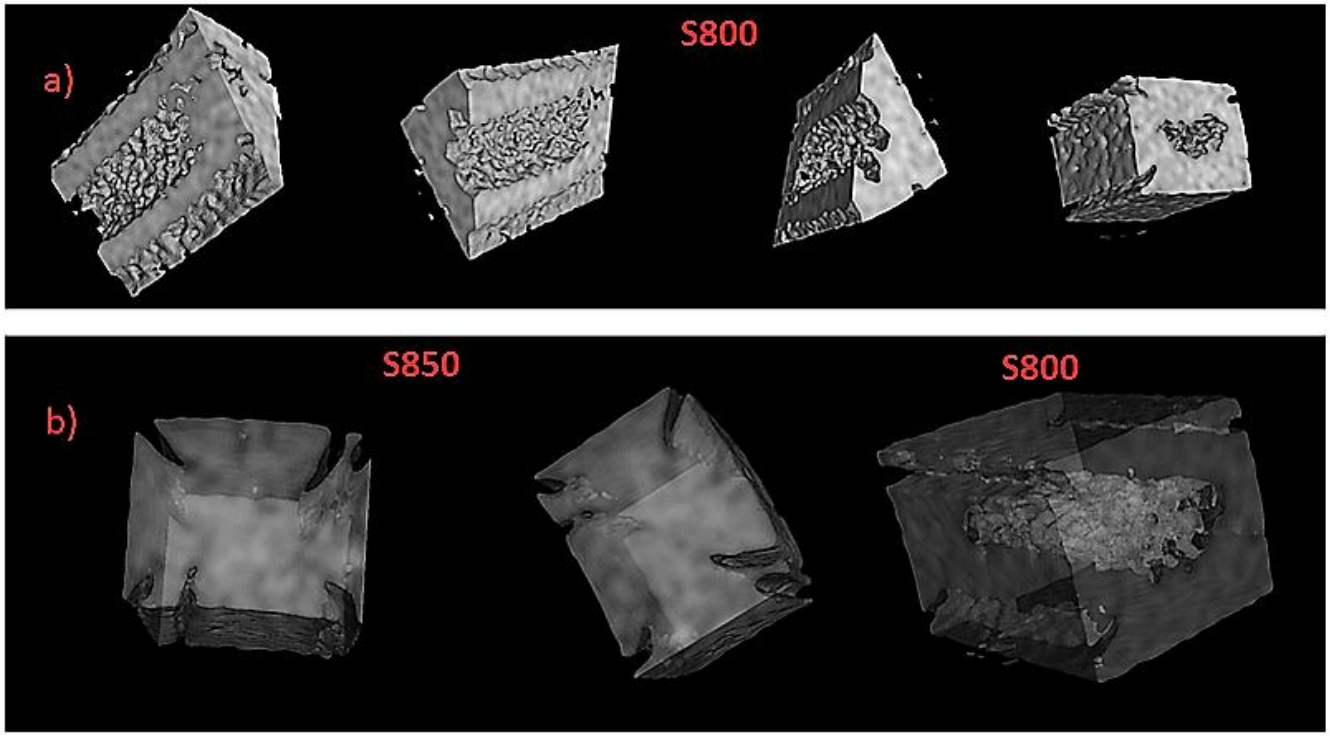
a)
S800
b)
S850
S800

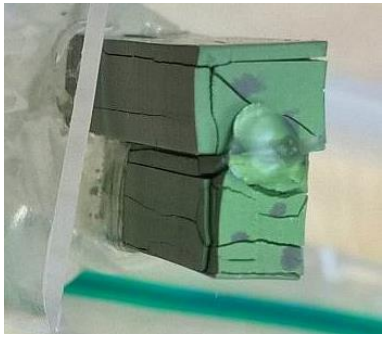

In-situ neutron imaging of red–ox cycling (at 800ºC) of anode supports for SOFC (BOA at PSI, Switzerland)

Initial oxidized state | After reduction | After oxidation | After reduction | After oxidation

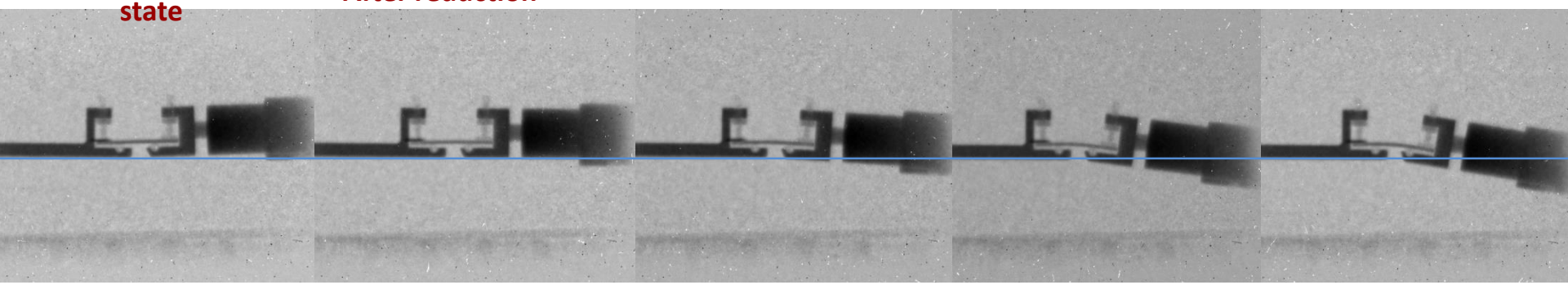

Initial oxidized state

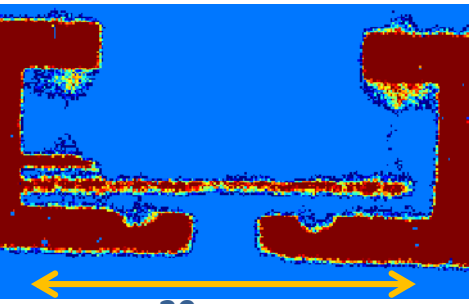

Reduced

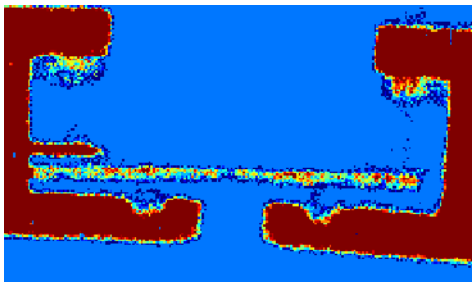

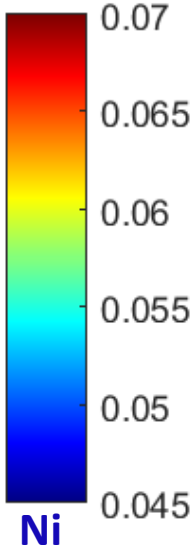

Macroscopic cross section [1/mm]

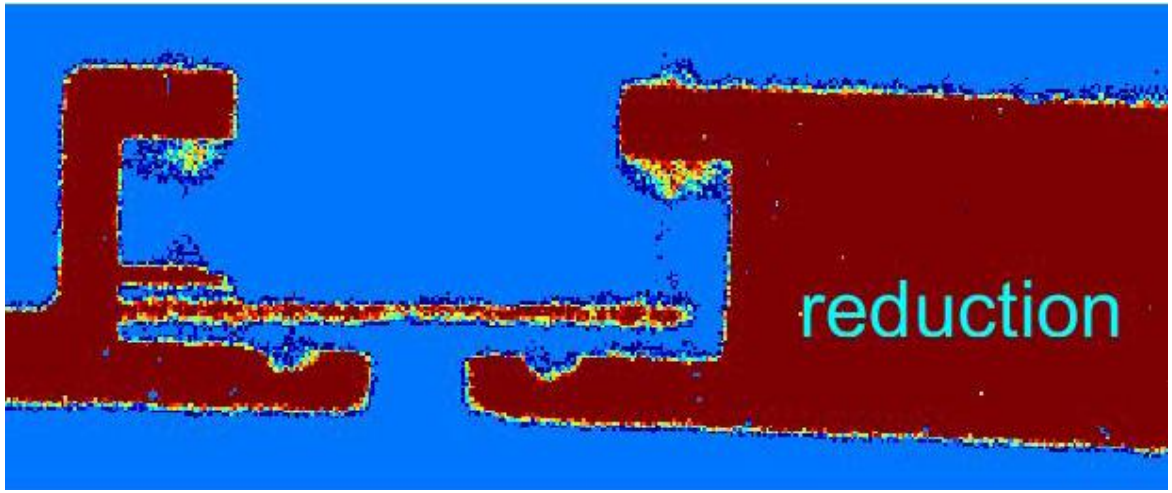

Anode supports with an electrolyte (RADEN)

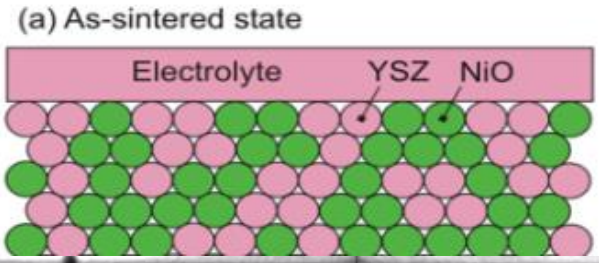

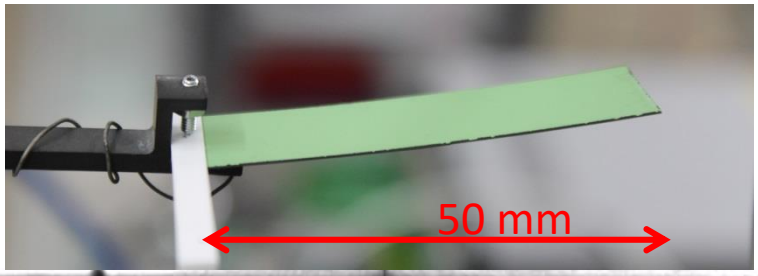

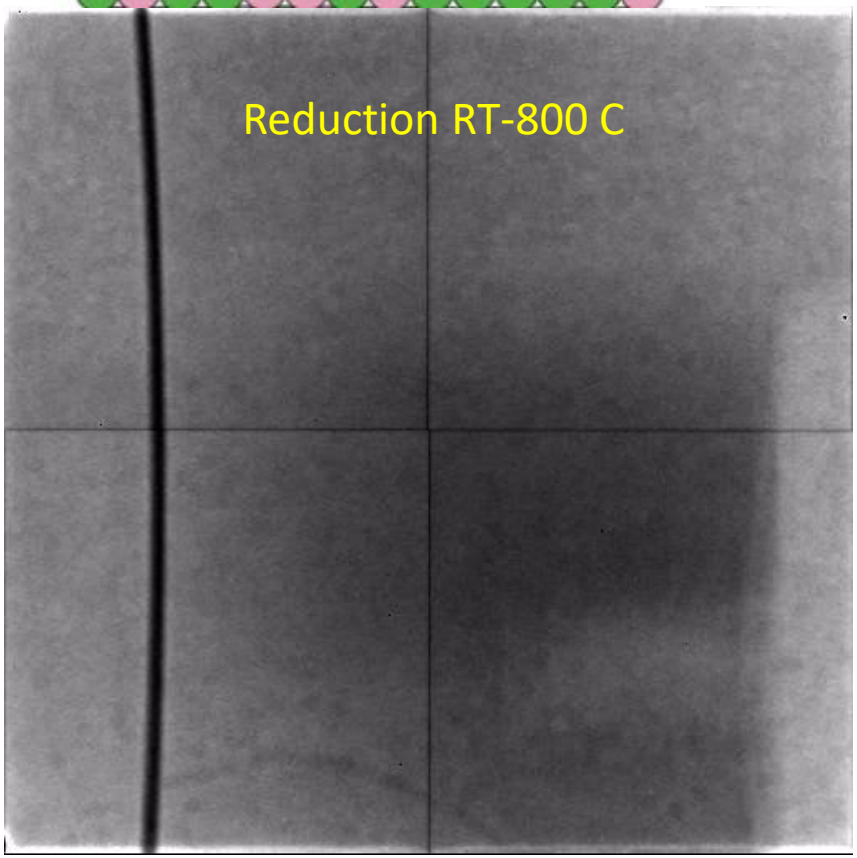

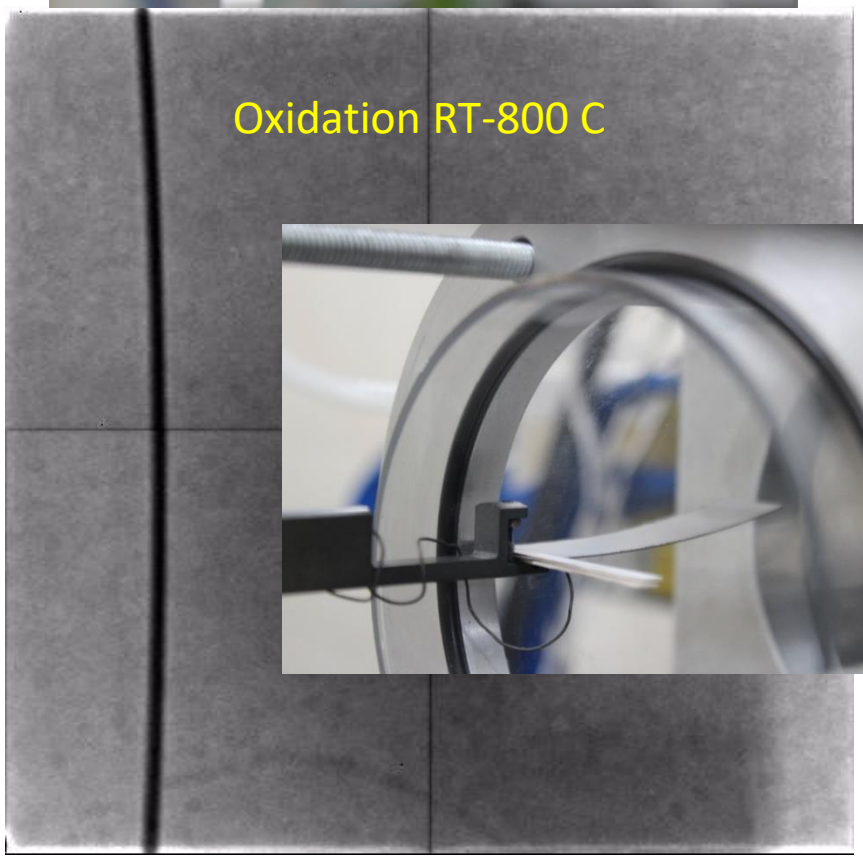

Anode supports with an electrolyte (RADEN)

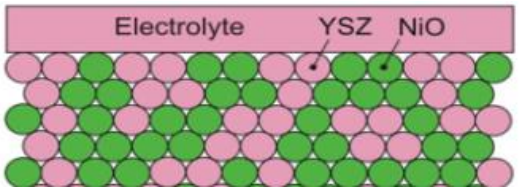

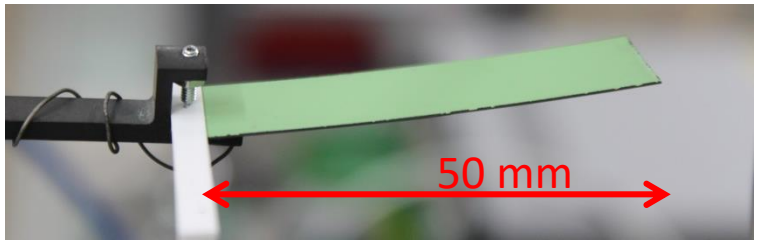

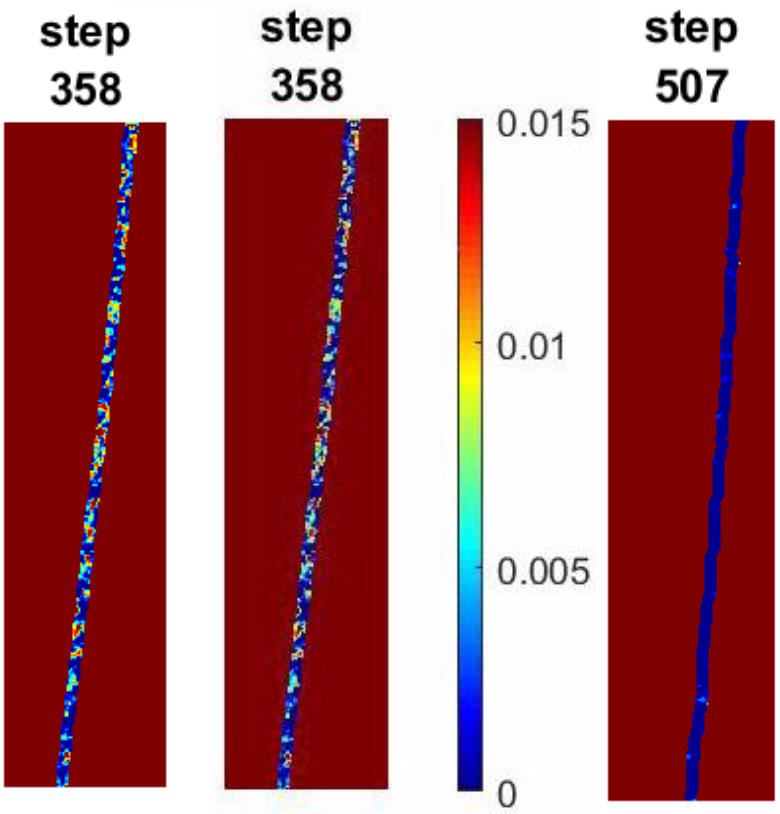

Reduction RT-800 C

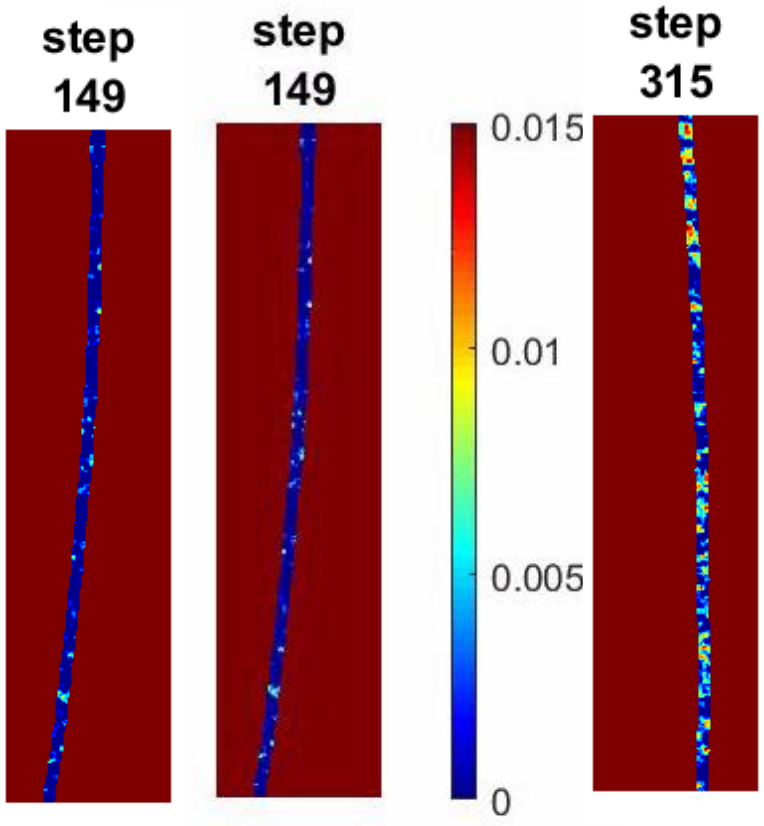

Oxidation RT-800 C

Phase transition in steel

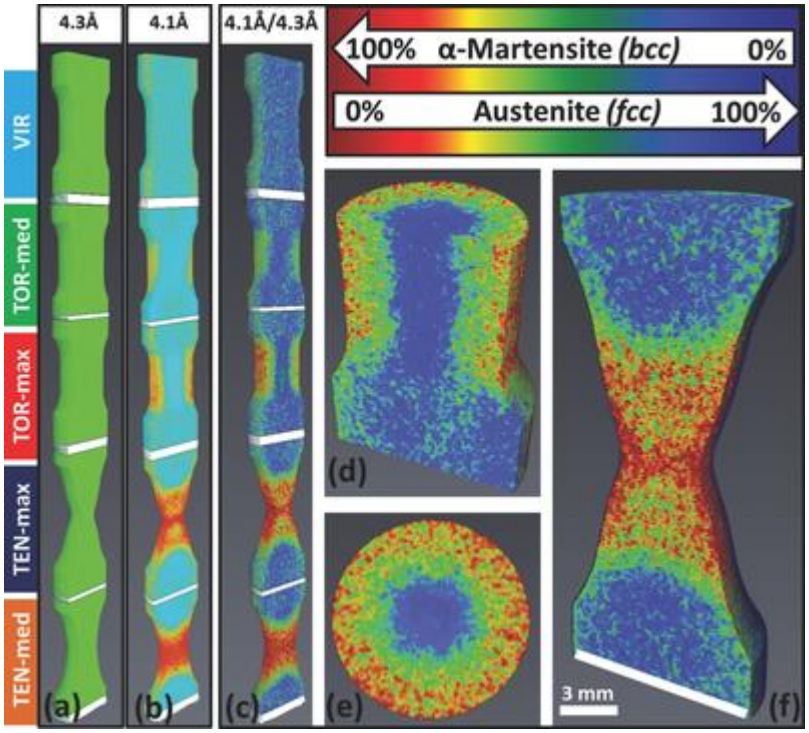

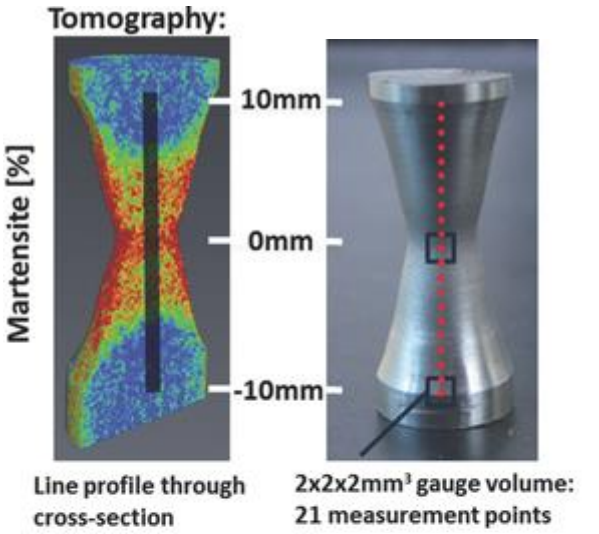

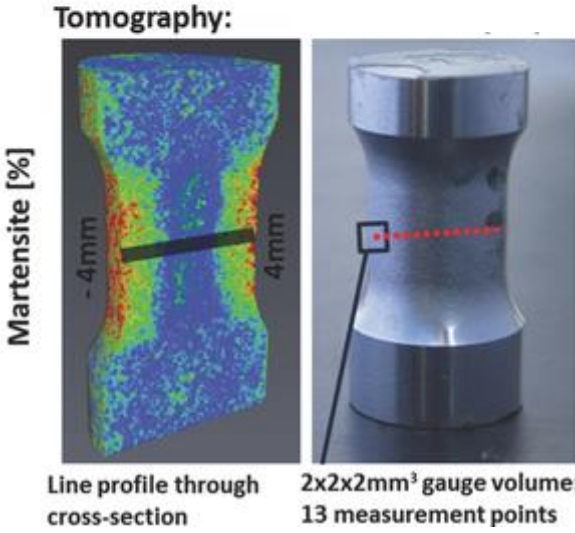

R. Woracek, D. Penumadu, N. Kardjilov, A. Hilger, M. Boin, J. Banhart, and I. Manke, "3D mapping of crystallographic phase distribution using energy-selective neutron tomography.," *Adv. Mater.*, vol. 26, no. 24, pp. 4069–73, Jun. 2014.

Strain mapping

$$\varepsilon = \frac{\Delta d_{hkl}}{d_{hkl}} = \frac{d_{hkl} - d0_{hkl}}{d_{hkl}}$$

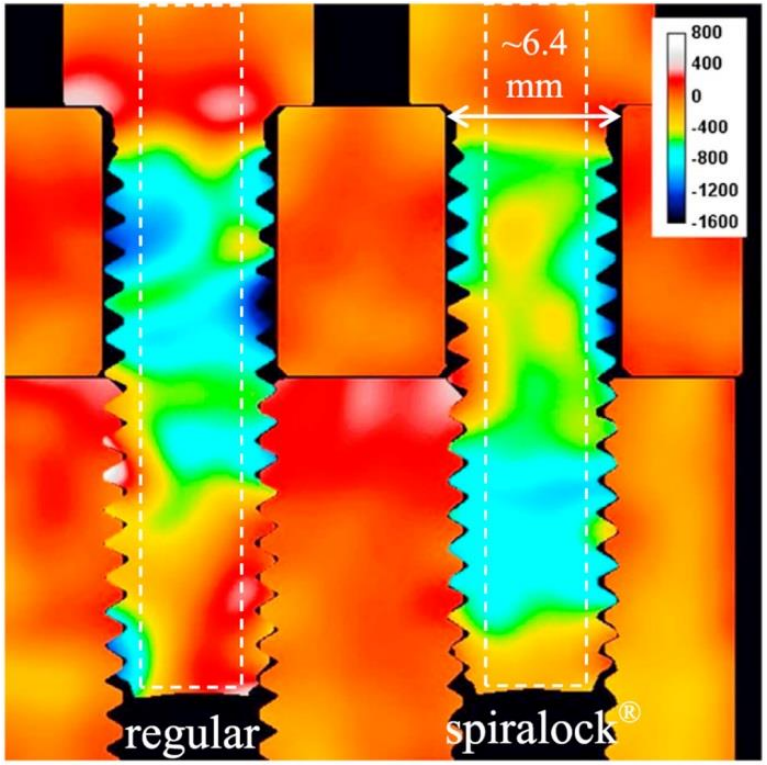

A. S. Tremsin, T. Y. Yau, and W. Kockelmann, “Non-destructive Examination of Loads in Regular and Self-locking Spiralock® Threads through Energy-resolved Neutron Imaging,” *Strain*, vol. 52, no. 6, pp. 548–558, Dec. 2016.

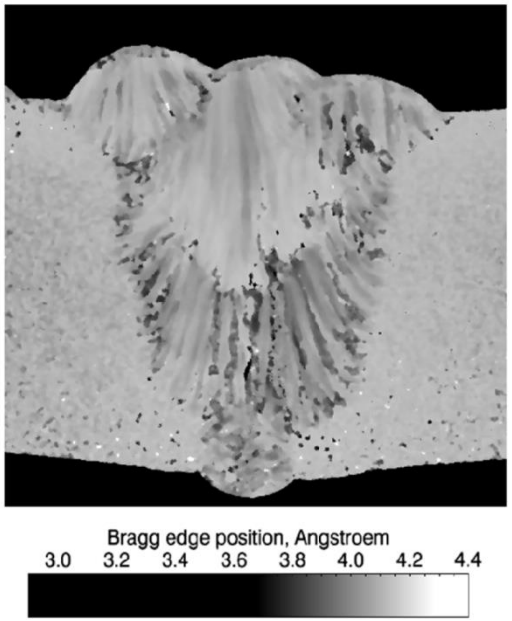

[N. Kardjilov, I. Manke, A. Hilger, S. Williams, M. Strobl, R. Woracek, M. Boin, E. Lehmann, D. Penumadu, and J. Banhart, “Neutron Bragg-edge mapping of weld seams,” *Int. J. Mater. Res. (formerly Zeitschrift fuer Met.*, vol. 103, no. 2, pp. 151–154, Feb. 2012.

Texture mapping

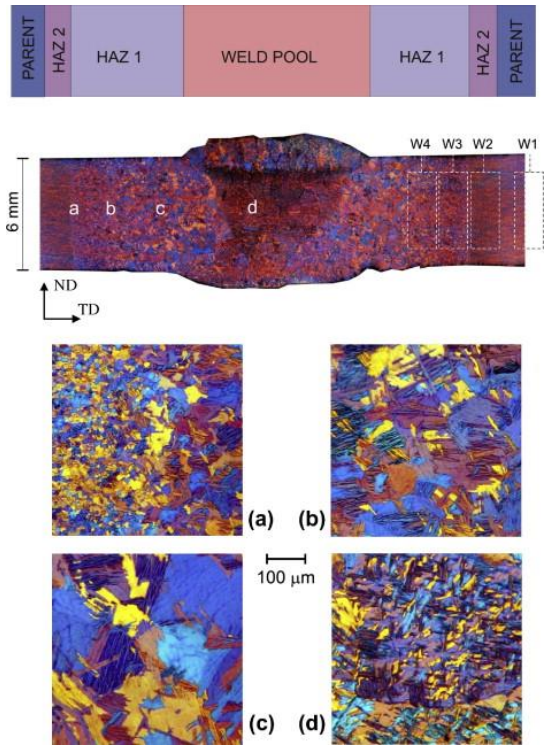

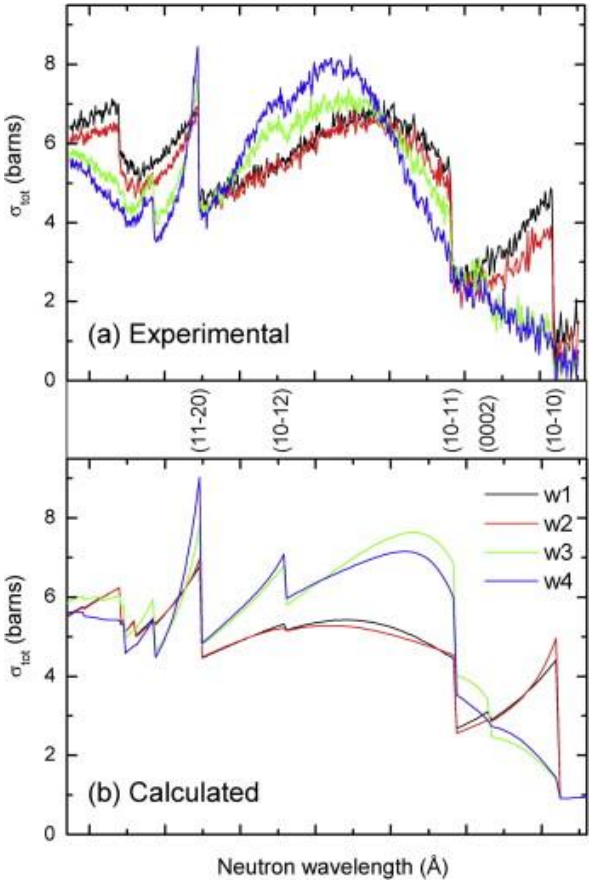

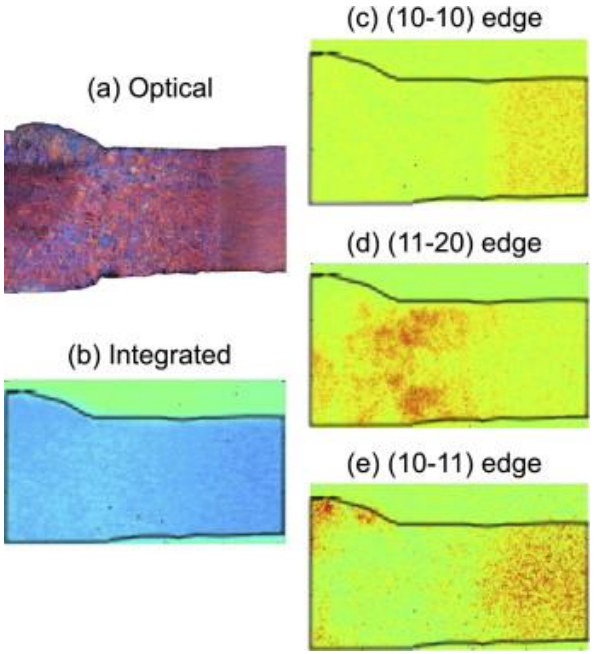

J. R. Santisteban, M. A. Vicente-Alvarez, P. Vizcaino, A. D. Banchik, S. C. Vogel, A. S. Tremsin, J. V. Vallerga, J. B. McPhate, E. Lehmann, and W. Kockelmann, "Texture imaging of zirconium based components by total neutron cross-section experiments," *J. Nucl. Mater.*, vol. 425, no. 1–3, pp. 218–227, Jun. 2012.

Now last but not least – applications in cultural heritage

→ next talk of Francesco Grazzi

Data analysis

- Nxs: A program library for neutron cross section calculations
- Imaging Bragg Edge Analysis Tool for Engineering Structure – iBeatles
- RITS code: Microstructure retrieval and full pattern refinement

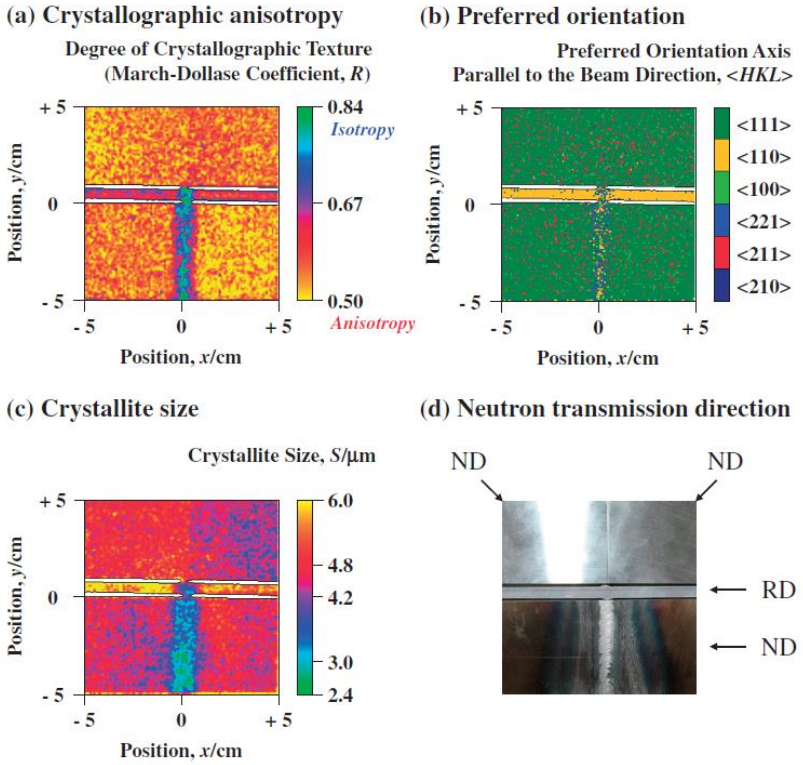

Fig. 9 Quantitative images of the information on the texture and the microstructure inside the α-iron plates. (a) Degree of the crystallographic anisotropy. (b) Preferred orientation axis that is parallel to the beam transmission direction. (c) Size of the crystallite where the primary extinction phenomenon occurs. (d) Neutron transmission direction in each specimen.

H. Sato, T. Kamiyama, and Y. Kiyanagi, "A Rietveld-Type Analysis Code for Pulsed Neutron Bragg-Edge Transmission Imaging and Quantitative Evaluation of Texture and Microstructure of a Welded α-Iron Plate," *Mater. Trans.*, vol. 52, no. 6, pp. 1294–1302, 2011.

In-situ phase analysis – averaging over ROI

4 min full ox, whole sample

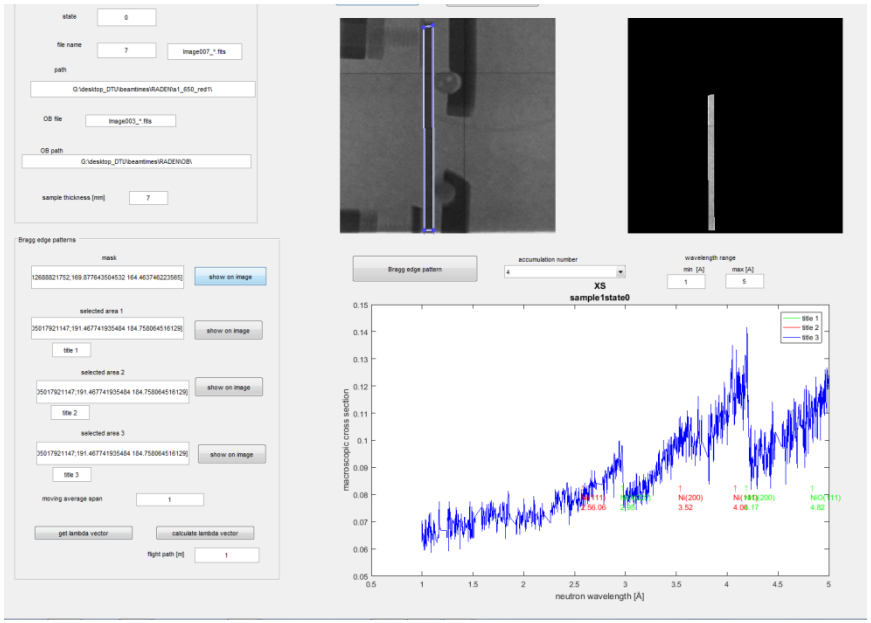

4 min full ox, small ROI

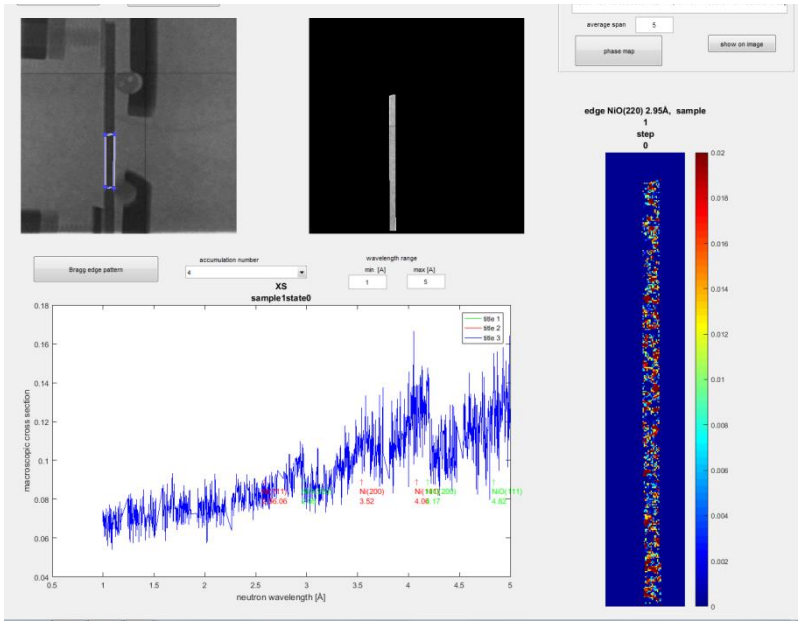

4 min full red, whole sample

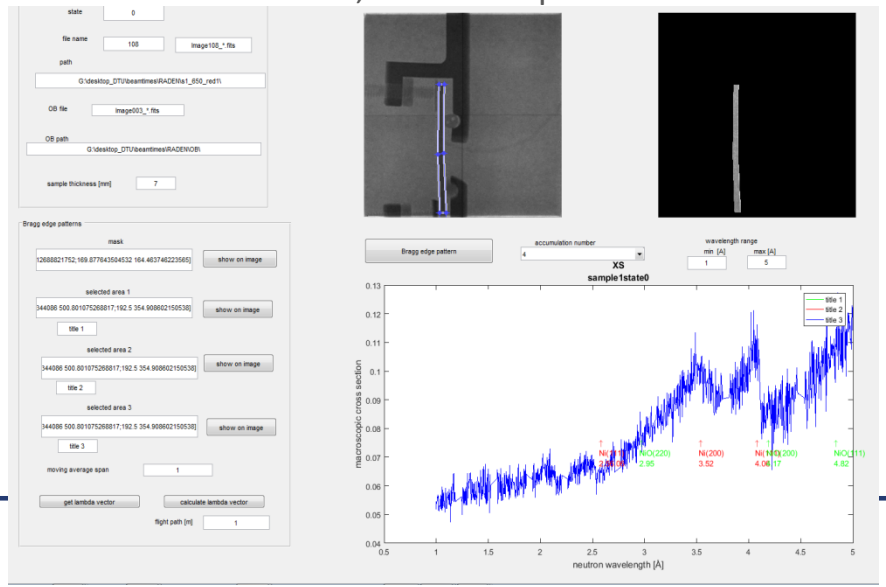

4 min full red, small ROI

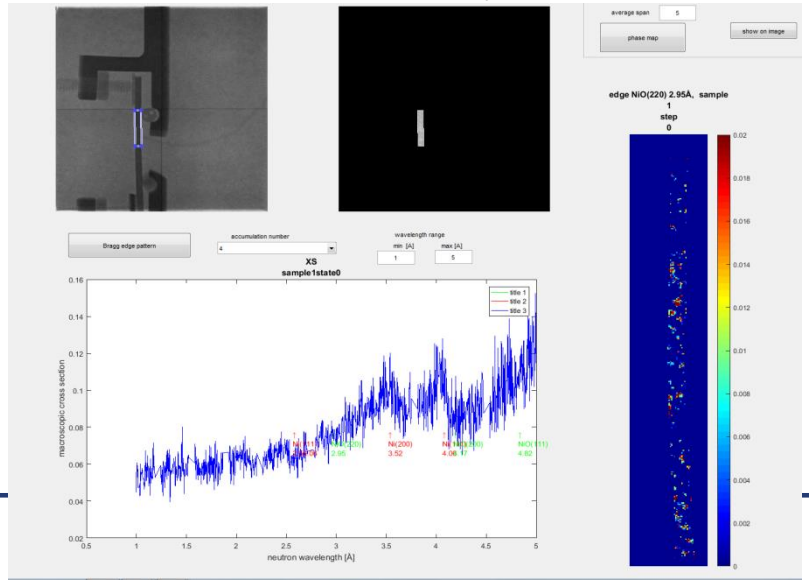

In-situ phase analysis – averaging over measurement time

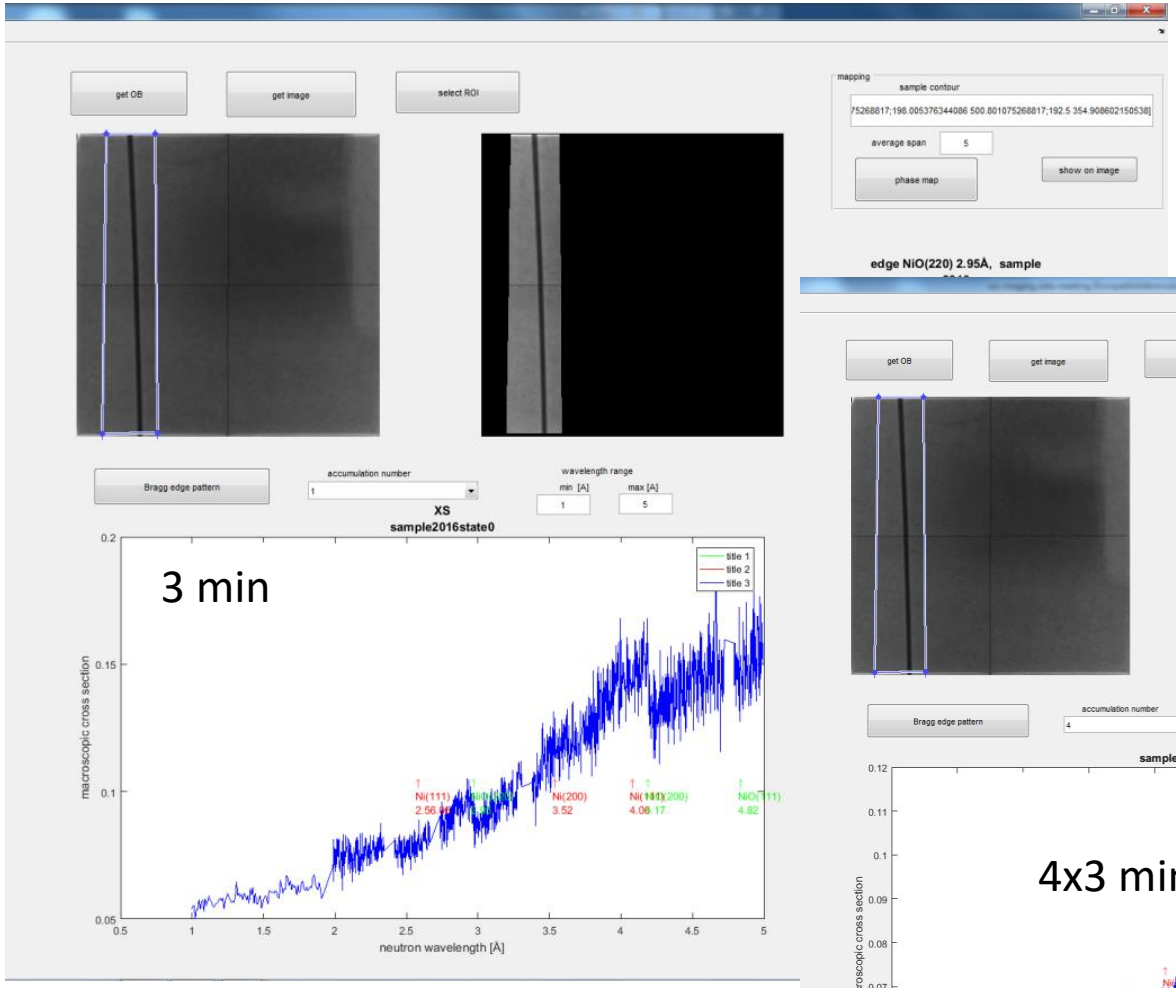

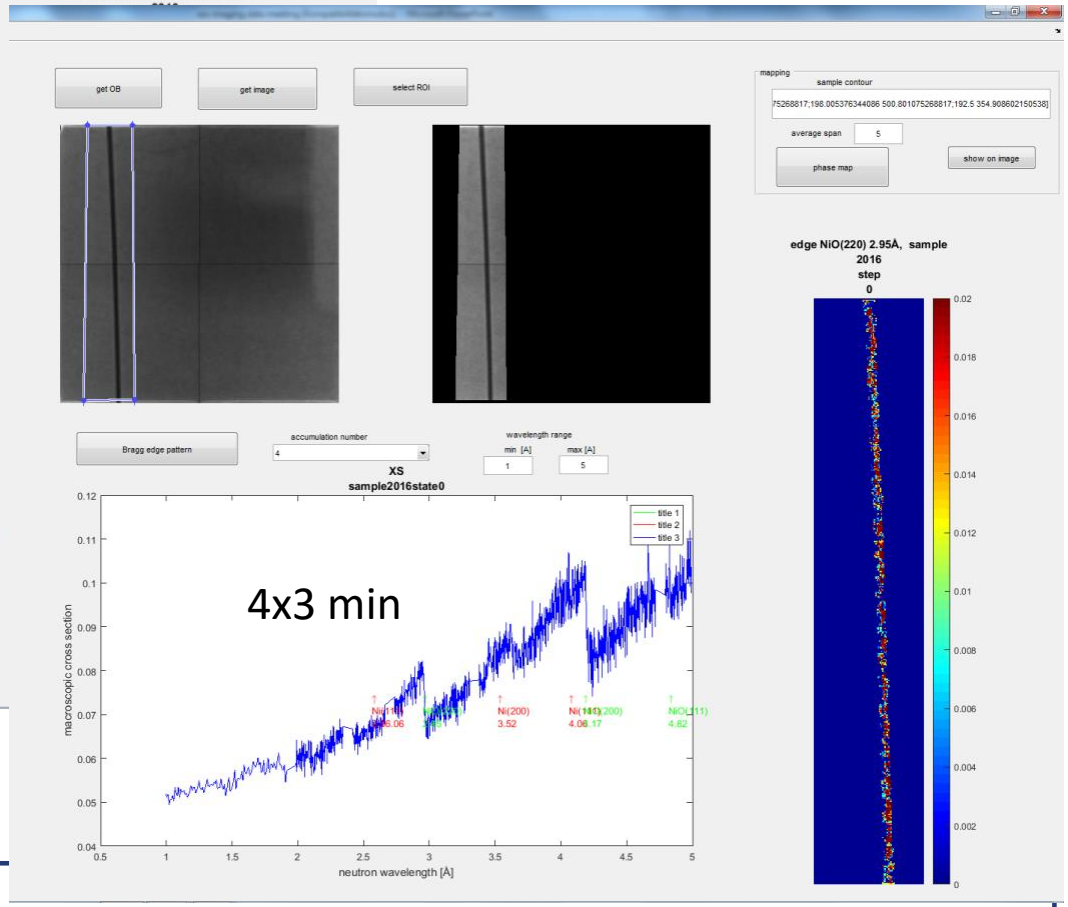

Averaging over TOF frames

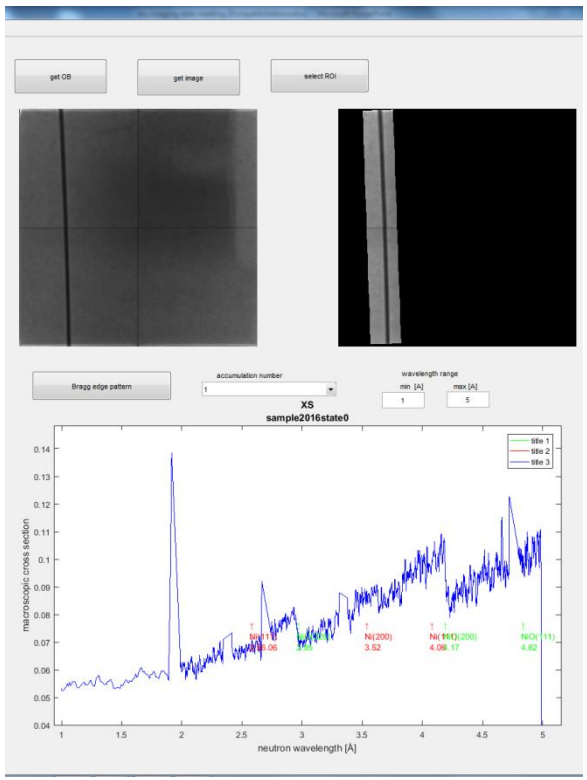

span 4

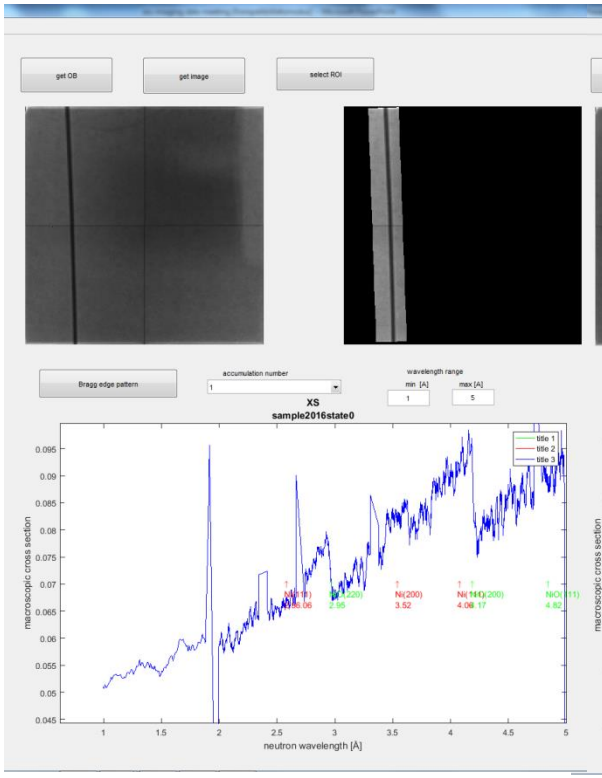

span 10

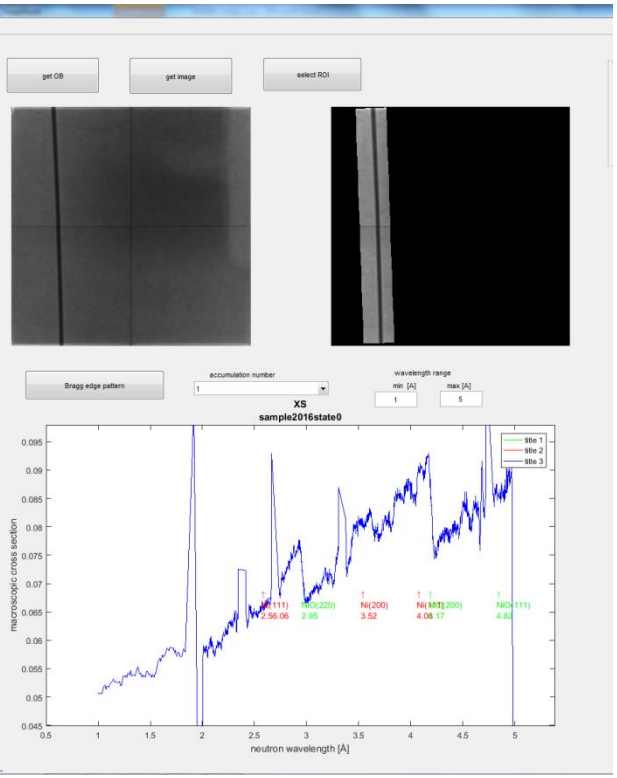

span 20

Further reading

- R. Woracek, J. Santisteban, A. Fedrigo, and M. Strobl, “Diffraction in neutron imaging—A review,” *Nucl. Instruments Methods Phys. Res. Sect. A Accel. Spectrometers, Detect. Assoc. Equip.*, 2017.
- W. H. Bragg and W. L. Bragg, “The Reflection of X-rays by Crystals,” *Proc. R. Soc. A Math. Phys. Eng. Sci.*, vol. 88, no. 605, pp. 428–438, Jul. 1913.
- S. Vogel, “A Rietveld-Approach for the Analysis of Neutron Time-Of-Flight Transmission Data,” Christian Albrechts Universitaet, 2000.
- J. R. Santisteban, L. Edwards, M. E. Fizpatrick, A. Steuwer, and P. J. Withers, “Engineering applications of Bragg-edge neutron transmission,” *Appl. Phys. A Mater. Sci. Process.*, vol. 74, pp. s1433–s1436, 2002.
- M. Boin, “Developments towards the tomographic imaging of local crystallographic structures,” no. February, 2011.

Thank you for your attention